Spectrochimica Acta Part A: Molecular and Biomolecular Spectroscopy 200 (2018) 158–166

Contents lists available at ScienceDirect

Spectrochimica Acta Part A: Molecular and Biomolecular Spectroscopy

journal homepage: www.elsevier.com/locate/saa

TCNQ molecular semiconductor of the Cu(II)TAAB macrocycle: Optical and electrical properties

M.E. Sánchez Vergara [a,*], R. Salcedo [b], Bertha Molina [c], R. Carrera-Téllez [a], J.R. Álvarez-Bada [a], A. Hernández-García [a], V. Gómez-Vidales [d]

[a] Facultad de Ingeniería, Universidad Anáhuac México, Avenida Universidad Anáhuac 46, Col. Lomas Anáhuac, Huixquilucan 52786, Estado de México, Mexico
[b] Instituto de Investigaciones en Materiales, Universidad Nacional Autónoma de México, Circuito Exterior s/n, Ciudad Universitaria, Coyoacán 04510, Ciudad de México, Mexico
[c] Facultad de Ciencias, Universidad Nacional Autónoma de México, Circuito Exterior s/n, Ciudad Universitaria, Coyoacán 04510, Ciudad de México, Mexico
[d] Instituto de Química, Universidad Nacional Autónoma de México, Circuito Exterior s/n, Ciudad Universitaria, Coyoacán 04510, Ciudad de México, Mexico

ARTICLE INFO

Article history:
Received 6 September 2017
Received in revised form 8 April 2018
Accepted 9 April 2018
Available online 11 April 2018

Keywords:
Semiconductor molecular material
DFT calculations
Thin film
Optical properties
Electrical properties

ABSTRACT

The present study reports the doping of a semiconducting molecular material through the formation of hydrogen bonds between the macrocycle Cu(II)(TAAB) and the electronic acceptor TCNQ. According to density functional theory (DFT) calculations and electron paramagnetic resonance (EPR) analysis, the doped compound has the shape of a distorted square pyramid, with four nitrogen atoms in the equatorial position and the apical oxygen atom from the water ligands. These water molecules can generate strong hydrogen bonds with TCNQ and the TAAB metallic complex. Thin films of copper molecular material were obtained through high vacuum evaporation and were structurally characterized by IR spectroscopy, EPR and scanning electron microscopy (SEM). Additionally, the absorption coefficient (α) and photon energy ($h\nu$) were calculated from UV–vis spectroscopy and used to determine the optical activation energy in each film, from which its semiconducting behavior was established. An important aspect to consider is that the presence of hydrogen bonds is essential to establish the semiconducting nature of these species; this chemical behavior, as well as the resulting electronic mobility, have been studied by DFT theoretical calculations, which reinforce the experimental conclusion of a relationship between Cu(II)TAAB and TCNQ moieties generated by a weak bond. Finally, *I–V* characteristics have been obtained from a *glass/ITO/doped molecular semiconductor/Ag* device using Ag and ITO electrodes. Results for the copper-based device show that, at low voltages, the conduction process is of an ohmic nature while, at higher voltages, space-charge-limited current (SCLC) is found. It is highly probable that the doping effect in TCNQ favors electronic transport due to the formation of conduction channels caused by dopant-favored anisotropy.

1. Introduction

Within the chemistry and physics of molecular materials, one of the most sought-after goals is the design, synthesis, and characterization of materials with interesting optical and electrical properties; this search received a great impulse with the synthesis of TTF-TCNQ (TTF = tetrathiafulvalene; TCNQ = tetracyanoquinodimethane), the first organic conductor [1–3]. From the discovery of the charge transfer complex TTF-TCNQ, research activity in the field of molecular conductors and semiconductors has readily increased [2], as they possess interesting electrical, optical and/or magnetic properties [2–4]; this is due to their low dimensionality, the formation of energy bands, and their ability to yield or accept electrons at a low energy cost, facilitated by the partial occupation of their energy bands. The degree of charge transfer, that is to say, the different occupation levels of the bands, significantly affects the electronic properties [4–6]. Thus, electrical conductivities similar to those of metals require that the width of the valence band be greater than the energy represented by the coulombic repulsion among the conduction electrons within a given molecule. Otherwise, electrons become localized in each molecule and the material behaves as a semiconductor. To get a low coulombic repulsion value, the molecules should be able to stabilize their associated charges, and for this, it is most appropriate for them to be polarizable with a heterogeneous distribution of charges. Additionally, and considering the desirability of stable solids, molecules should be capable of forming stable radicals (such as TTF and TCNQ, which act as π-electron donor and acceptor, respectively) [1–5], with valence electrons located above and below the median plane of the molecule in delocalized π orbitals.

One of the groups of compounds that form stable radicals with π-delocalized electrons is that of metal complexes with ligands derived from *o* aminobenzaldehyde tetra anhydrotetramer $M(II)(TAAB)^{2+}$ [7], which constitutes a specific class of molecular materials in which the ligand and metal exert a profound influence on the electrical, optical and

* Corresponding author.
E-mail address: elena.sanchez@anahuac.mx. (M.E. Sánchez Vergara).

https://doi.org/10.1016/j.saa.2018.04.021
1386-1425/

magnetic properties [7–9]. These complexes are formed by the self-condensation of *o* aminobenzaldehyde [7,10] in the presence of transition metallic ions such as Ni(II) and Cu(II), which are capable of acting as templates [11]. The metal complexes of $M(II)(TAAB)^{2+}$ have provided unusual examples of isomerism and one-dimensional assemblies [7,9] that permit different types of molecular arrangements involving conduction channels, which are associated to a marked anisotropy in the material, especially when they are in thin-film form. As mentioned above, the 16 members of the cyclotetrameric macrocyclic-complexes category have a delocalized electronic structure [12]. Around the macrocyclic cation, the coordination sphere next to the metallic atom is almost flat; nevertheless, the general geometry of the macrocyclic complex shows an S_4-symmetric saddle form, i.e., it can be described as a hyperbolic paraboloid [13]. The structure and its properties will depend on the anion to which it is attached; for instance, in $Ni(TAAB)X_2$ complexes, when X^- is ClO_4^- or BF_4^-, there is a flat square geometry for nickel; when X^- is NO_3^- or I^-, compounds have a tetragonal geometry. The incorporation of substituent groups in the macrocyclic binder is of considerable interest, because of the possibility of using such systems as organic semiconductors in the manufacture of optoelectronic devices, of which organic field-effect transistors (OFETs), organic light-emitting diodes (OLEDs) and organic solar cells (OSCs) are significant examples among a wide variety of products using organic semiconductors.

This work refers to the doping effect of a semiconducting molecular material formed by $[Cu(II)(TAAB)]^{2+}$ and the TCNQ electronic acceptor. The doped semiconductor was deposited as a thin film and structurally characterized and its optical and electrical properties were evaluated to determine the material's usability as organic semiconductor in optoelectronic devices. Weak noncovalent interactions determining the structure of an organic semiconductor imply that the environment of each molecule may not be identical to those of other molecules, affecting the electronic structure of the semiconductor. Taking this consideration into account, the electronic behavior of this material has been compared with results obtained from theoretical calculations. Theoretical results match well with the corresponding experimental behavior and many features can be explained from them.

2. Experimental and Instrumentation

7,7,8,8 Tetracyanoquinodimethane was obtained from Sigma-Aldrich and required no further purification. Nitrate of [tetrabenzo (*b,f,j,n*){1,5,9,13}tetraazacyclohexadecine] copper(II): $[Cu(BzO_4[16]octaeneN_4)](NO_3)_2$ macrocycle was prepared according to Labuda et al. [12]. The molecular material was doped by a simple reflux between $[Cu(II)(TAAB)]^{2+}$ and TCNQ derivatives. It is important to mention that Inoue et al. [8] synthetized the semiconductor complex $Cu(TAAB)(TCNQ)_n$ ($n = 1.5$ or 2) from the metathesis between lithium tetracyanoquinodimethanide, Li(TCNQ), and the copper chelate with tetrabenzo[*b,f,j,n*][1,5,9,13]tetraazacyclohexadecine. In this work, the doping process is different from that stablished by Inoue [8], and was carried out through hydrogen bonding between the TCNQ molecule and the $[Cu(II)(TAAB)]^{2+}$ macrocycle (see Scheme 1), so that TCNQ may be used as the neutral molecule and not necessarily as the anion.

2.1. Preparation of Doped Molecular Semiconductor

204 mg (1 mmol) of TCNQ in 10 ml absolute methanol was added to 600 mg (1 mmol) of $[Cu(BzO_4[16]octaeneN_4)](NO_3)_2$ previously dissolved in 30 ml of absolute methanol. The mixture was kept under reflux for three days and the solid thus obtained was filtered and washed with a 1:1 methanol-water solution, in order to remove "free" amounts of both starting materials, and dried in vacuum. Elemental analysis was performed in an Exeter Analytical CE-440 model. Calculated analysis for $C_{52}H_{30}N_{14}O_7Cu$: C, 60.80; H, 2.92; N, 19.10. Experimental analysis: C, 61.04; H, 2.83; N, 18.81. An excess of any component in the mixture could influence charge transport properties and is unintended. However, it must be noted that, according to the elemental analysis that was carried out, the doped semiconductor has impurities, probably due to the nitro radical of the precursor, as was corroborated by means of IR spectroscopy. A combination of elemental analysis and IR spectroscopy was used to study the structure of doped semiconductor [14–16]. Taking into account that most molecular semiconductors are used as films in device manufacturing, the doped semiconductor was subsequently deposited using the high-vacuum evaporation technique. Because of its thermal stability, the powdered material was heated to 573 K in order to produce a phase change to the gaseous state, so that it could finally be deposited in thin-film form upon contact with substrates which were at room temperature and a vacuum of 1×10^{-5} Torr. The substrates used for deposition were indium tin oxide (ITO) coated glass slides, high-resistivity monocrystalline n-type silicon wafers (c-Si), Corning glass and quartz. Substrates were previously submitted to a sonication cleaning process with different solvents and were dried under an argon flow. IR spectroscopy was carried out in order to verify the vibrational modes of the organic radicals that integrate the molecular material. The IR analysis was carried out using a Nicolet iS5-FT in KBr pellet and with the film deposited on silicon wafers. The EPR measurements were made in a quartz tube at 77 K, using a Jeol JES-TE300 spectrometer operating in the X-Band, with 100 kHz modulation frequency and cylindrical cavity in the TE_{011} mode. The external calibration of the magnetic field was made with a Jeol ES-FC5 precision gauss meter operating in the microwave band with frequency counter 5350B HP. The spectrometer settings for all spectra were as follows: centerfield 300 ± 75 mT; microwave power 1 mW, microwave frequency 9.02256 GHz, modulation width 0.079 mT; time constant, 0.1 s; amplitude 50; sweep time 120 s. Spectral acquisition, manipulation and simulation were performed using the program ES-IPRIT/TE, v1.916. The EPR spectrum was recorded at a first derivation and default values for the main parameters, including the g-factor values. For SEM, a ZEISS EVO LS 10 scanning electron microscope was operated at a voltage of 20 kV and a focal distance of 25 mm, using a thin film on a quartz substrate. The X-ray diffraction analysis was performed using the θ-2θ technique with a Bragg-Brentano Rigaku ULTIMA-IV diffractometer and working with CuK-α ($\lambda = 0.15405$ nm) radiation on a Corning glass substrate. Thickness values were obtained through profilometry measurements on silicon substrates, with a Bruker profilometer, DEKTAK XT model, with STYLUS, LIS 3, 2 μm RADIUS-Type B. The optical absorption of the thin film on the quartz substrate was measured with a Unicam spectrophotometer, model UV300, in the wavelength range of 200–1100 nm. UV–vis spectroscopy was carried out to determine the electronic transitions, as well as measurements related to the intramolecular and intermolecular bands, which are those that provide more information about the valence state of the organic radicals. The glass/ITO/*doped molecular semiconductor*/Ag devices were fabricated by deposition processes, under the same conditions of temperature and pressure as for its precursor. Electrical conductivity measurements were performed by using the four contacts, or wires, method, in which the electric current is passed through the end wires, and the potential difference between the central wires is measured. For the electrical characterization of the device, a programmable voltage source, a sensing station with lighting and a temperature controller circuit by Next Robotix, as well as an auto-ranging Keithley 4200-SCS-PK1 pico-ammeter, were employed.

3. Theoretical Methods

All geometries were optimized using a pure DFT method for energy evaluation, applying Becke's gradient corrections [17] for exchange and Perdew-Wang's parametrization for correlation within the local density approximation [18]. This is the scheme for the B3PW91 method that forms part of the Gaussian 09 Package [19]. All calculations were performed using the 6-31G** basis set. Frequency calculations were carried out to confirm that the optimized structures were at a minimum of the

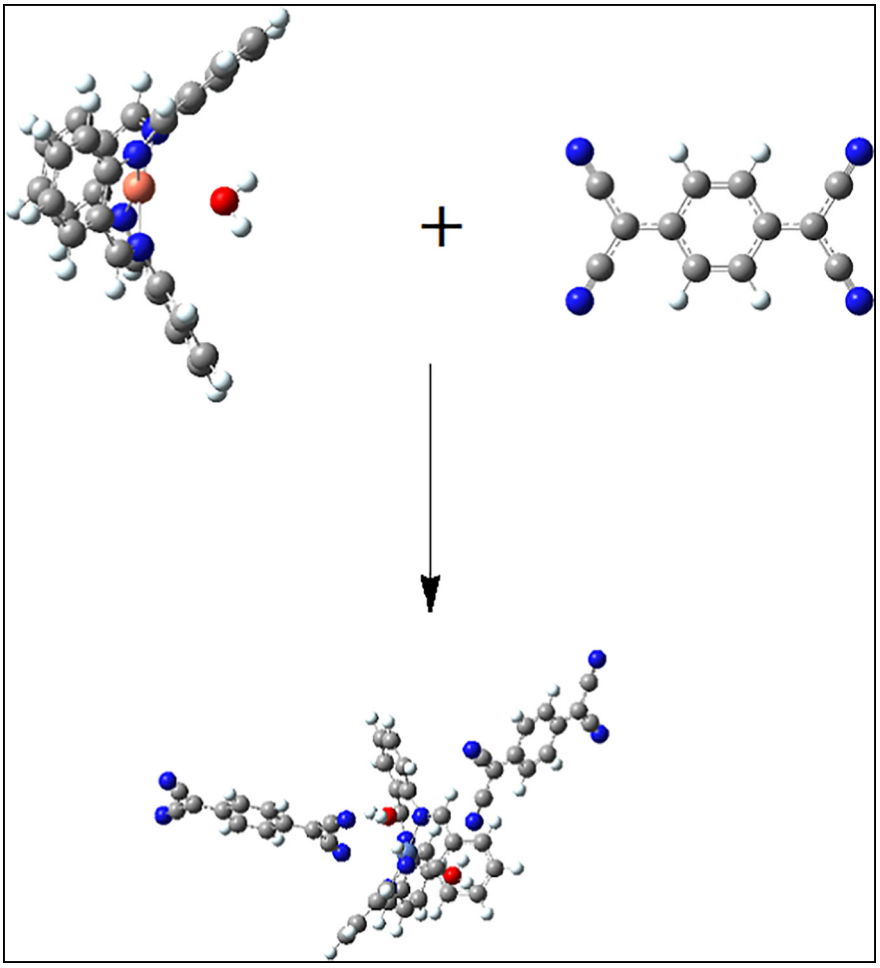

Scheme 1. The interaction between TAAB and TCNQ which yields the complex containing hydrogen bonds. In the illustration the grey atoms correspond to carbon, blue to nitrogen, red to oxygen and white to hydrogen.

potential surfaces. The hydrogen bonds were studied with the Grimme module (G3) implemented in the Gaussian09 package [20].

4. Results and Discussion

According to Bansal et al. [21] the $[Cu(BzO_4[16]octaeneN_4)]^{2+}$ macrocycle attains its saddle-shaped geometry due to the presence of four phenyl rings. Due to this geometry, the vacant axial sites in such macrocycle complex facilitate the link with small molecules, like the water molecule or anions. IR spectroscopy (see Table 1) confirms the presence of the expected bonds in KBr pellets for the molecular semiconductor in powder form, and on the silicon substrate for the deposited film. Four absorption bands are observed around 1614, 1589, 1494 and 1442 cm^{-1}; referring to the elongation vibration of the ortho-disubstituted benzenes in the macrocycle. On the other hand, an intense and acute band is also found around 1566 cm^{-1}, which is attributed to the C═N elongation mode of the imine group. The presence of the band due to C═N vibrations indicates that the macrocycle did not suffer alteration in its most sensitive group, as previously reported by Katovic and Taylor [10] in their work on nucleophilic addition reactions in $[M(TAAB)]^{2+}$ compounds, where the imine groups are introduced as the sensitive regions of the macrocycle. The above suggests that the TCNQ was not directly linked to the metallic ion, but through water molecules [22]. In addition, C≡N stretching bands of TCNQ appeared around 2224, 1668, 1446, and 1206 cm^{-1} and, below the edge of the electronic absorption band, two weak but unmistakable bands were observed around 838 and 829 cm^{-1} in the CH bending region [8,22]. Finally, there are three bands in the spectrum, whose position and form correspond to the O—H asymmetric stretch, symmetric stretch and bend vibrations around 3413, 2124 and 1546 cm^{-1} respectively; these bands are due to the presence of water molecules in the doped semiconductor. Table 1 shows that the precursor $[Cu(II)(TAAB)]^{2+}$ lacks those bands related to the O—H bond indicative of water molecules; nevertheless, the doped molecular material does have them. This is an

Table 1
IR data for the doped molecular semiconductor and $Cu(II)(TAAB)^{2+}$ precursors.

Sample	ν (C_6 ring) (cm^{-1})	ν(C═N) (cm^{-1})	ν(O—H) (cm^{-1})	ν(C≡N) (cm^{-1})	ν(C—H) (cm^{-1})
$[Cu(BzO_4[16]octaeneN_4)](NO_3)_2$ Pellet	1609, 1592, 1496, 1443	1565	–	–	–
$[Cu(II)(TAAB)(H_2O)](TCNQ)_2$ Pellet	1612, 1586, 1492, 1442	1566	3416, 2124, 1545	2222, 1666, 1447, 1204	839, 829
$[Cu(II)(TAAB)(H_2O)](TCNQ)_2$ Thin film	1619, 1589, 1492, 1442	1567	3410, 2124, 1547	2226, 1669, 1445, 1209	836, 829

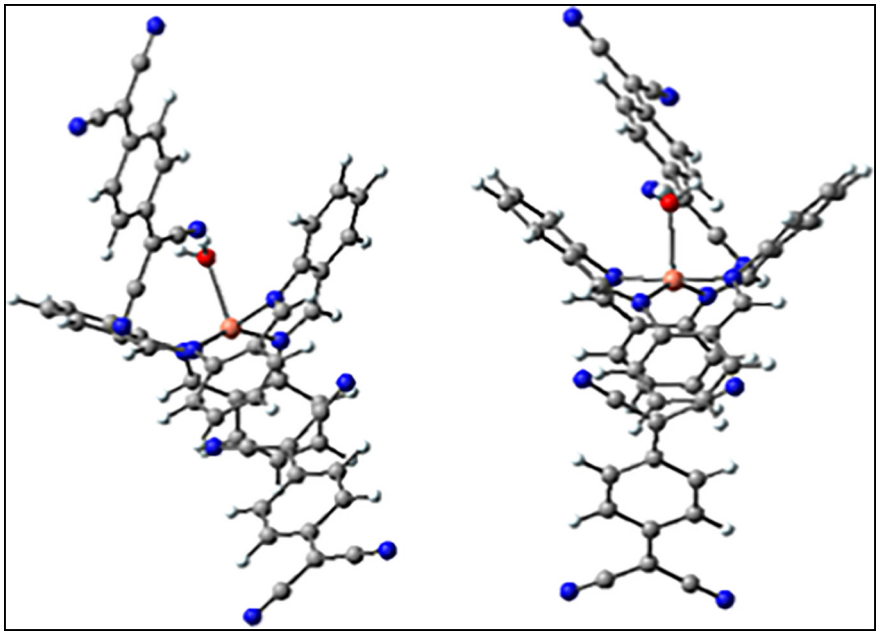

Fig. 1. Two views of the geometrical structure of the *[Cu(II)(TAAB)(H$_2$O)](TCNQ)$_2$* complex. Color code: pink-copper; blue-nitrogen; red-oxygen; dark grey-carbon; light grey-hydrogen.

indication of probable formation of hydrogen bonds between the macrocycle and TCNQ [22]; these results were supported by theoretical calculations. It must be taken into consideration that in the IR spectrum of the doped semiconductor, as well as in that of its precursor, there are bands related to the NO_3^{-1} ion from the precursor around 832, 1360 and 1387 cm^{-1}. The foregoing indicates that the doping process is not completely efficient and some impurities could remain, whose effect may be considered negligible, provided that they do not significantly affect charge transport.

4.1. Theoretical Study

The general structure of the doped material corresponding to the *[Cu(II)(TAAB)(H$_2$O)](TCNQ)$_2$* semiconductor is shown in Fig. 1. There are several points to note. First, the central framework of the molecules resembles a ruffle; however, the geometry of the polyhedron (considering the central atom as the origin of coordinates) is similar to a deformed square pyramid when considering only the metal atom, the coordinated nitrogen atoms and the apical water ligand. The water ligand has bond lengths of 2.5 Å approximately, which agrees with previous results [23]. The Cu(II) atoms are coordinated to the four nitrogen atoms of the macrocycle in an equatorial way (in common with the organic fragment of TAAB) and to the oxygen atom belonging to the water molecule in the axial position. Second, the water ligand can generate strong hydrogen bonds with other species, and this is indeed the case when the interaction between TCNQ and the $[Cu(II)(TAAB)]^{2+}$ derivative is considered. All the hydrogen bonds among the TAAB complex and both TCNQ molecules are shown in Fig. 2, whereas the bond lengths appear in Table 2.

The calculations show a large thermodynamic stabilization in the formation of this molecular material; the system has an energy difference of −94.55 kcal/mol, favoring the complex against the separated copper macrocycle and TCNQ molecules. This phenomenon can be seen as the conformation of a kind of donor-acceptor complex [24], the given energy difference accounting for all the hydrogen bonds. It is evident that there are short bonds which are stronger than other bonds, but the calculated energy difference is very important to establish the free TAAB molecule attraction to the TCNQ moieties.

Another interesting point is that it is possible to find at least eight hydrogen bonds of different types. The first and the stronger one is that

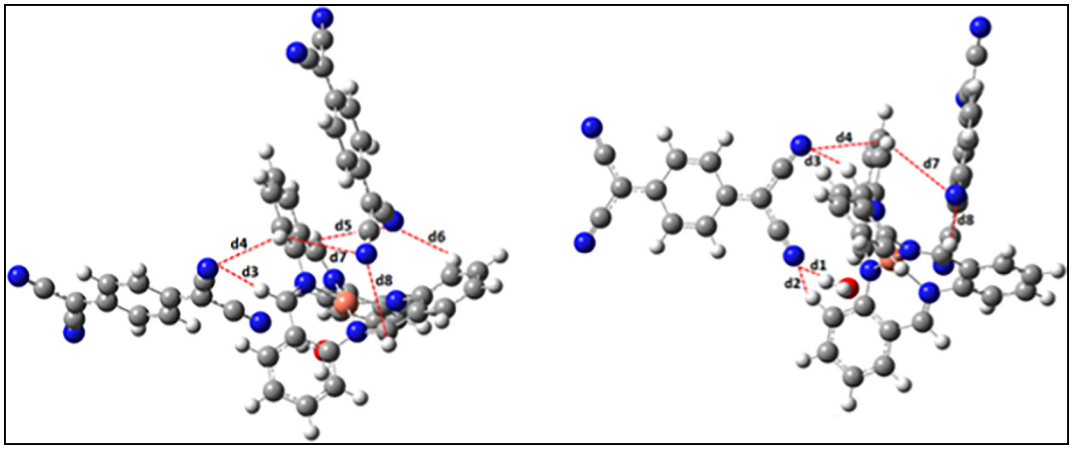

Fig. 2. Schematic structure of *[Cu(II)(TAAB)(H$_2$O)](TCNQ)$_2$*. The red-dotted lines mark the eight hydrogen bonds within TCNQ.

Table 2
Bond lengths between the TAAB complex and the TCNQ molecules.

	UB3PW91	UB3PW91-GD3
$\Delta E_{HL\alpha}$ (eV)	2.24	2.355
$\Delta E_{HL\beta}$ (eV)	2.24	2.373
d1 (Å)	1.867	1.866
d2 (Å)	2.909	2.865
d3 (Å)	2.678	2.376
d4 (Å)	2.447	3.332
d5 (Å)	2.767	3.429
d6 (Å)	2.437	2.828
d7 (Å)	3.203	3.331
d8 (Å)		3.587

formed between the apical water ligand and the terminal nitrogen atoms coming from the lateral cyano groups of the TCNQ molecule; the length of this interaction is 1.867 Å, a very short distance for a bridge of this kind. This strong bond is the one suggesting the formation of a molecular adduct. Almost all the other hydrogen bonds arise from the interaction between one of the terminal hydrogen atoms from the outer phenyl ring of the TAAB macrocycle and the same terminal nitrogen atom of the TCNQ moiety (see Fig. 2); in this case, there are several different length values, as it is noted from Table 2, and there are even weak bonds between one terminal hydrogen from water and both TCNQ molecules. The description of the resultant complex is very important because its shape is related to the electronic behavior of this species. The central ruffle is attracted by both TCNQ moieties in two different ways. The first TCNQ is attracted to the water molecule and establishes a very strong interaction (the strongest for the whole set of hydrogen bonds), while the other one is attracted to the free region below the molecule (i.e. the base of the pyramid), perhaps as if it were about to form a covalent bond to occupy the sixth position. Several hydrogen bonds are formed in this situation, however, precluding a shorter interaction. This particular situation leads to a rather jammed electronic-transit zone.

An atomic-molecular analysis [25] of our species reveals that its hydrogen bonding can be considered as a multicenter, proton-acceptor σ type in all cases, except for the interaction between the hydrogen atoms from the water ligand and the nitrogen from TCNQ, which is a one-center proton acceptor according to the classification by Grabowski [26]. The possible hydrogen interactions which account for the stabilization of the crystal cell were not included in the present study because they require a new methodology capable of accounting for all the interactions in these systems, which will be the subject of future work.

The electronic behavior of the compound is illustrated by the nature of its frontier molecular orbitals. Fig. 3 shows the shapes of the lowest-unoccupied (LUMO) and singly-occupied (SOMO) molecular orbitals. These shapes arise from the open-shell (doublet multiplicity) electronic distribution, which yields the Cu(II) ion. The LUMO has the same form in the α, as well as β, contributions, as they essentially constitute a complete molecular orbital without energy changes. It is worth noticing that this function is completely focused on one of the TCNQ moieties, i.e. the electrons flow to the best electron acceptor fragment;

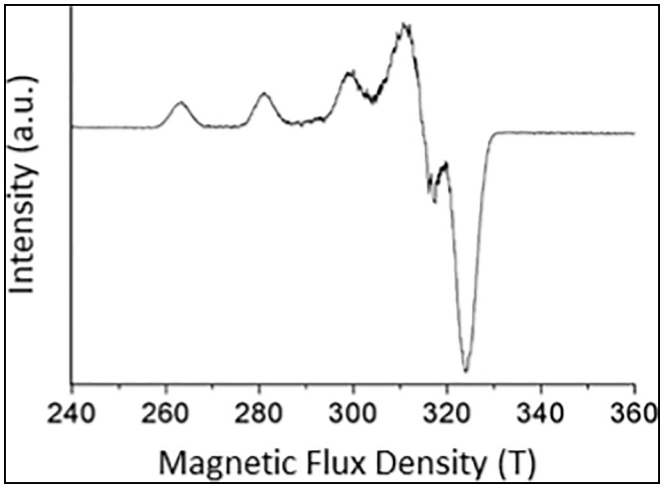

Fig. 4. EPR spectrum of *[Cu(II)(TAAB)(H$_2$O)](TCNQ)$_2$* in MeOH at 77 K.

meanwhile, the SOMO (which contains the single electron) is delocalized between the same moiety of the TCNQ molecule and the center of the TAAB macrocycle involving the copper atom and its bonds with the neighboring nitrogen atoms. The pathway for electronic transit shows that the delocalized single electron at the center of the TAAB macrocycle can reach only one TCNQ molecule, leading to the formation of a conducting pair complex. The energy gap calculated between HOMO and LUMO is 2.38 eV, a result that suggests a semiconducting behavior.

4.2. EPR Results

Electron paramagnetic resonance is the spectroscopic technique of choice for the study of copper complexes. With this technique, it is possible to determine the electronic flux around the copper(II) ion [27–29], and obtain information about its complex geometry. This technique also provides information about the occupation of paired and unpaired orbitals. When the complex is in the ground state, the occupation of the $d_{(x^2-y^2)}$ atomic orbital and an axial symmetry pattern $g_{||} \gg g_{\perp} > 2.0023$ are expected, while a $d_{(z^2)}$ configuration yields an inverse axial symmetry $g_{\perp} \gg g_{||} \approx 2.0023$. The EPR spectral analysis of [Cu(BzO$_4$[16]octaeneN$_4$)](NO$_3$)$_2$ and *[Cu(II)(TAAB)(H$_2$O)](TCNQ)$_2$* in frozen-glass (77 K) MeOH solution showed complexes with axial symmetry. The trend in g-values suggests that the unpaired electron in copper(II) occupies the $d_{(x^2-y^2)}$ orbital. In these conditions, all EPR spectra show characteristic, monomeric-copper(II) complexes with hyperfine lines associated to coupling of the unpaired electron in the copper ion with its nuclear spin ($I_{Cu} = 3/2$). The superhyperfine structure due to the coupling with the nitrogen atom ($I_N = 1$) is not well resolved (Fig. 4 shows the intensity of the EPR spectrum as a function of the magnetic flux density, which is linearly proportional to the magnetic field intensity).

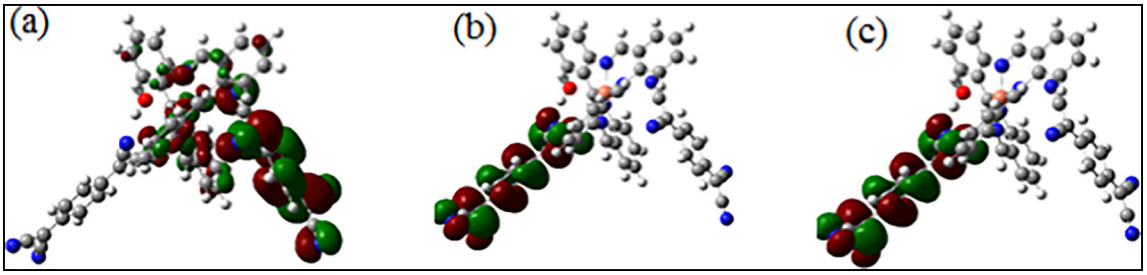

Fig. 3. Frontier molecular orbitals for *[Cu(II)(TAAB)(H$_2$O)](TCNQ)$_2$*: (a) SOMO, (b) LUMO-α and (c) LUMO-β.

Table 3
EPR mesurements.

Sample	$g_{\|}$	$g_{\perp}$	$A_{\|}$	$A_{\perp}$	A_{iso}	g_{iso}
$[Cu(BzO_4[16]octaeneN_4)](NO_3)_2$ 17022301	2.225	2.047	18.04 187.4	0.8 7.6	67.5	2.1064
[Cu(II)(TAAB)(H_2O)](TCNQ)$_2$ 17022302	2.2258	2.047	17.90 186.00	0.8 7.6	67.09	2.1066

A_{iso}, $A_{\|}$, $A_{\perp}$ ($\times 10^{-4}$ cm^{-1}).

The constants g and A were obtained by simulation and are shown in Table 3, which also provides the calculated values of A_{iso} and g_{iso} for these complexes in frozen solution. They are in the range of values previously attributed to complexes with a square-based pyramidal geometry [30,31]. The molecule has the shape of a distorted square pyramid with four nitrogen atoms in the equatorial position and the apical oxygen atom from the water ligand. All the information in Table 3 corresponds to the description of an open-shell species. The shape of the spectrum reinforces the argument for the copper complex having an unpaired electron. EPR results do not provide evidence of charge-transfer transitions, such as MLCT/LMCT.

4.3. Optical and Electrical Properties

In order to study the optical and electrical properties and their possible applications in optoelectronics, a thin film of the doped semiconductor molecular material was prepared. Regarding the SEM analysis performed on the thin film (see Fig. 5), a homogeneous morphology without holes is observed in the 33× microphotograph shown in Fig. 5a. In order to analyze the general morphology of the film, the observation was made considering the smallest increase in which the thin film is visualized in the microscope (33× in this case) and subsequently analyzed at 10000×, to visualize the detail of the morphology of the film. This observation is relevant, as semiconductor thin films are required to be uniform in order for electric charge transport to be efficiently carried out [32,33]. High-vacuum evaporation, which was carried out for thin film formation, is a procedure that involves phase transitions in the molecular semiconductor due to significant thermal variations; this can cause both chemical degradation and the deposition of heterogeneous films. Nevertheless, the chemical and thermal stability of this material allowed optimum evaporation and deposition in this case, which is a fundamental requirement for a regular distribution of material along the whole substrate. Film homogeneity favors charge carriers' mobility and electrical conductivity, as they can move quickly from one molecule to another without dispersing or being trapped in structural irregularities [32–34]. The absence of thin film irregularities prevents the dissipation of electromagnetic radiation, which may be a concern if the film is intended to be used in the manufacture of optoelectronic devices, such as OSCs [32,34]. The doped semiconductor film is formed by the agglomeration of round particles (Fig. 5b shows one such particle at 10000× magnification). It seems that, during the deposition of molecular material on the substrate, the heterogeneous nucleation processes directly depend on the structure of the molecule and the thermic gradient between the substrate (at 298 K) and the molecular material (at 573 K). Due to the lower free energy per unit volume of the sphere, the nuclei of molecular material deposited on the substrate resemble this geometry, which is maintained as the deposit advances and the film grows. In order to supplement these results, X-ray diffraction (XRD) was carried out in the film to enhance the morphological analysis of the molecular material arrangement deposited in film form. Fig. 6 shows an XRD trace of the doped semiconductor film. It can be noticed that this is essentially an amorphous structure, for the film only produced first-order peaks. This implies that evaporation and film deposition lead to desalination of the molecular structure. During the deposition process, when the molecules reach those regions of the substrate at lower temperatures, their kinetic energies become insufficient for them to have enough surface mobility. Long-reach order is thus not achieved and a structure with very little crystallinity results. This low crystallinity does not necessarily limit the semiconductor character of the molecular material, with short-range order exerting more influence on electronic behavior than long-range disorder.

UV–vis spectroscopy was performed in order to analyze the different electronic transitions taking place between the ground state and the excited state, as a consequence of radiation absorption at varying wavelengths. The results for the doped semiconductor and the precursor are shown in the electronic spectra of Fig. 7a. In the precursor case, no relevant signals are observed in the spectrum; however, the presence of the TCNQ molecule and hydrogen bonds significantly increase such signals in the doped case. From its spectrum, the doped film has absorption maxima located at wavelengths 407, 444 and 467 nm [35]. The absorption band observed above the 407 nm feature is attributable to $\pi \rightarrow \pi^*$ transitions within a macrocycle ring [36]. Intense absorption bands were observed at 444 and 467 nm; they suggest that hydrogen bonding between one of the terminal hydrogen atoms from the outer phenyl ring of the TAAB and the terminal nitrogen atom of the TCNQ moiety (see Fig. 2) produces strain in the CuTAAB skeleton [36]. The spectrum from the doped semiconductor extends into longer wavelengths which could, to some extent, be related to d-d transitions of the ion. Other electronic transitions lead to a broad band around 525 nm which is generated by the presence of TCNQ in the molecular material [37]. The absorption spectrum for this material is located essentially in the blue-violet range, which indicates that this compound would be practically transparent to IR and could perhaps find use in some optoelectronic devices.

The most remarkable characteristics of the doped molecular semiconductor arise from the electronic delocalization along its π-conjugate structure. In the molecular aromatic skeleton of electronic donor and acceptor, each carbon atom has three orbitals with sp^2 hybridization, which are distributed within the same plane around the same atom. Besides, each carbon atom possesses a p_z orbital, which is

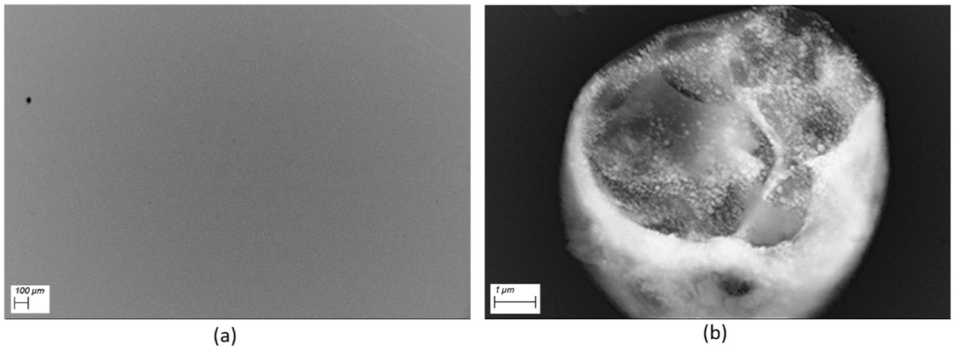

Fig. 5. SEM images of (a) the semiconductor film at 33× and (b) a particle within the semiconductor molecular film at 10000×.

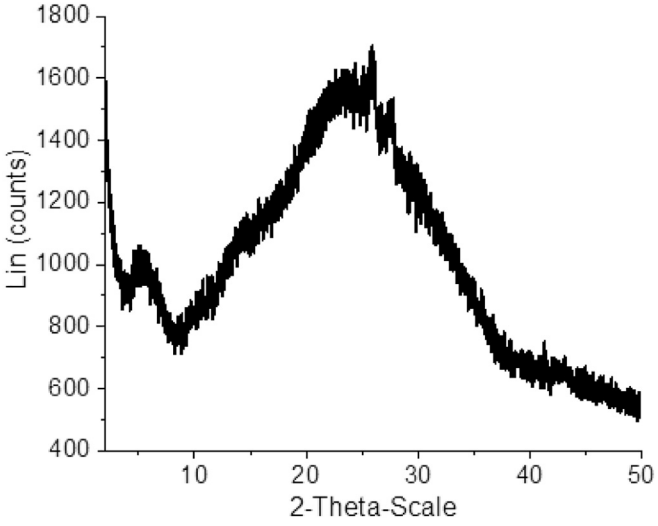

Fig. 6. XRD pattern of doped semiconductor film.

perpendicular to the sp^2 orbital plane. Therefore, the basic structure of each aromatic skeleton consists of σ bonds, because of the overlapping between sp^2 orbitals, and π bonds, due to the overlapping of p_z orbitals. This overlapping leads to a lower-energy bonding π orbital and a higher-energy anti-bonding π^* orbital which are those that respectively contribute to the valence band HOMO and the conduction band LUMO. The energy difference between these two bands is known as the *band gap* and is possible to assign it a value from the optical activation energy of the E_g, band, calculated from the absorption UV–vis spectrum and Tauc's semi-empirical model [38]. The optical band gap defines the nature of electroluminescent activity in OLEDs and light absorption efficiency in OSCs. The Tauc band gap associated with the films is determined through an extrapolation of the linear trend observed in the spectral dependence of $(\alpha h\nu)^{1/2}$ over a limited range of photon energies $h\nu$ (Fig. 7b) [39]. The absorption coefficient α near the band edge shows an exponential dependence on photon energy, usually obeying the Urbach relation $\alpha h\nu = \beta(h\nu - E_g)^n$, where $n = 1/2$ is a number characterizing the indirect transition process in amorphous semiconductors [39]. During thin-film formation, materials undergo considerable thermal gradients, which causes structural disarray and an amorphous film structure (see Fig. 6). Table 4 shows the parameters determined for both samples. E_g for molecular materials has typical values between 1.5 and 4.0 eV, so the results obtained are within the expected range [34]. The presence of TCNQ in the material slightly reduces the band gap (see Table 4); thus, the conductivity of the thin film is expected to increase. The theoretical value of the band gap (2.38 eV) is

Table 4
Characteristic parameters of *[Cu(II)(TAAB)(H$_2$O)](TCNQ)$_2$* and its precursor.[a]

Sample	*t* (nm)	E_g (eV)	σ_{298K} ($S\cdot cm^{-1}$)
glass/ITO/[Cu(BzO$_4$[16]octaeneN$_4$)](NO$_3$)$_2$/Ag	163	2.6	1.49
glass/ITO/[Cu(II)(TAAB)(H$_2$O)](TCNQ)$_2$/Ag	343	2.4	5.39

[a] *t*: film thickness; σ: electrical conductivity; E_g: band gap.

very similar to the one obtained by Tauc's model for the doped molecular material (2.4 eV); ideally, for the use of these semiconductor films in optoelectronic devices, a band gap of less than 1.8 eV would be expected [34]. The films do not fulfill this requirement, but it is necessary to consider that the separation of HOMO and LUMO energy levels also depends on structural factors in the material, such as the alternation in bond length and the degree of stacking of the electron donor and acceptor molecules [34]. The evaluation of the *I–V* behavior of the material provides complementary information to establish the usability or non-usability of this molecular material in optoelectronic applications.

The application of semiconductor molecular materials to different classes of devices involving more than one compound, such as the case presented in this work (Cu(II)TAAB and TCNQ derivatives), requires that a general characterization of the device be made to provide relevant information regarding the behavior of the material for device use, as well as for manufacturing purposes. To determine the electrical behavior of the semiconductor material presented here, a bulk heterojunction-type glass/ITO/*doped molecular semiconductor*/Ag structure was built, using a glass substrate with a layer of the ITO transparent conductor, which has a random texture and acts as a front contact or anode, while the back contact or cathode was formed with a reflecting Ag layer. For the electrode construction, it was taken into account that those materials that are prone to hole injection behave as anodes, while those prone to electron injection behave as cathodes. A bulk heterojunction structure was chosen, due to the active layer that is formed by the Cu(II)(TAAB) macrocycle and the TCNQ when joined by hydrogen bonds, which provides a larger contact surface and higher excitonic diffusion [40]. Additionally, the presence of hydrogen bonds avoids the short-circuiting of the device by defining regions for selective percolation of the charge carriers to the correct electrode. After the device was built, its electrical characteristics were measured and the *I–V* relationship was analyzed to characterize the electrical behavior of the devices. To carry out the *I–V* behavior evaluation, a collinear measurement was carried out by applying four linearly arranged tips of equal spacing to the two devices (1.59 mm), with a current being applied to the outer tips, and a voltage measured at the inner tips. Fig. 8 shows the *I–V* characteristics at room temperature for the precursor device (Fig. 8a) and the doped molecular device (Fig. 8b) under the effect of different types of electromagnetic radiation in the wavelength range

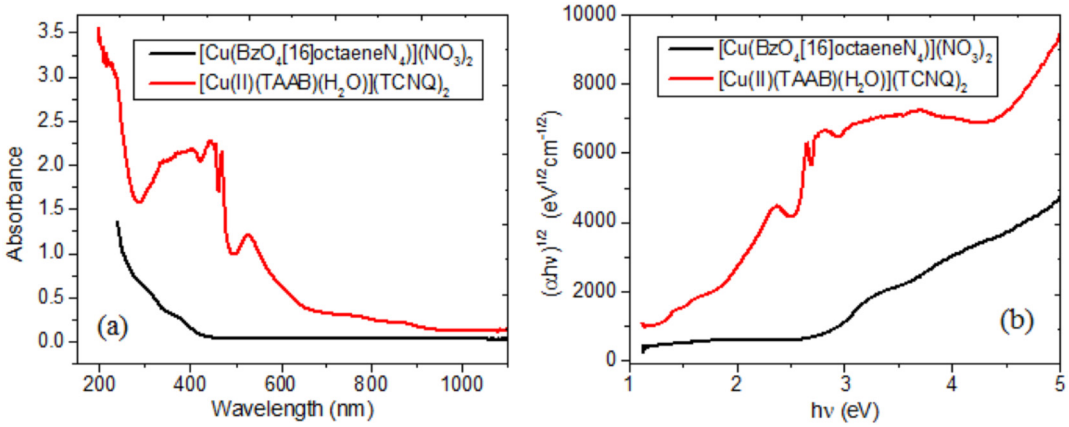

Fig. 7. (a) Electronic spectra and (b) Tauc plot of *[Cu(II)(TAAB)(H$_2$O)](TCNQ)$_2$* and precursor [Cu(BzO$_4$[16]octaeneN$_4$)](NO$_3$)$_2$ films.

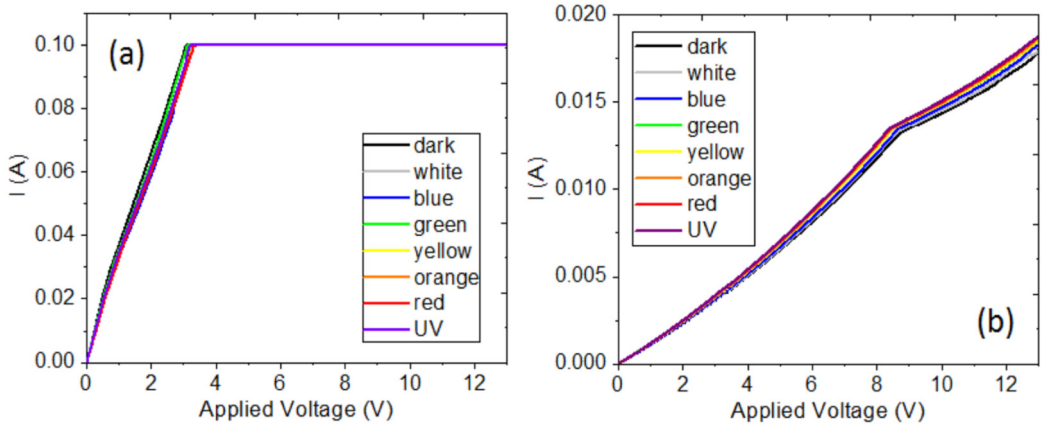

Fig. 8. *I–V* heterojunction measurements for (a) *[Cu(BzO$_4$[16]octaeneN$_4$)](NO$_3$)$_2$*, (b) *[Cu(II)(TAAB)(H$_2$O)](TCNQ)$_2$*.

between IR and UV, through visible radiation. It is worth mentioning that, according to Fig. 8, radiation seems to have no effect in electric charge transport; in all cases, the same current intensity was observed. This is important because, if one intends to use these molecular materials in the manufacture of devices such as OLEDs or OFETs, electrical transport should not be affected by the incident electromagnetic radiation; on the other hand, their usefulness in the manufacture of OSCs would be limited. The characterization of a photovoltaic device is carried out by taking *I–V* measurements both in dark conditions (in which case, the operation of the device would be analogous to that of a rectifying diode), and in artificial lighting conditions simulating the irradiation of the device by sunlight. When comparing the electrical transport of the precursor heterojunction structure glass/ITO/*Cu(II)(TAAB)*/Ag device with that of the doped semiconductor structure glass/ITO/*[Cu(II)(TAAB)(H$_2$O)](TCNQ)$_2$*/Ag (Fig. 8a/b), a practically ohmic behavior at low voltages is found in both cases but, in the case of the intrinsic semiconductor, it is followed by saturation at about 3 V, whereas the doped semiconductor has a space-charge limited conductivity (SCLC) current change for applied voltages above 8 V. The doped semiconductor in glass/ITO/*[Cu(II)(TAAB)/(H$_2$O)](TCNQ)$_2$*/Ag behaves as a resistor with low charge mobility; the slope in the *I–V* curve becomes smaller at higher field intensities, which could be related to some form of charge trapping within the SCLC regime. The macrocycle in this structure shows a significant orbital overlap because of the spatial extent of the transition metal *d*-orbitals. The variations observed in the magnitude of the electric current may be caused by the TCNQ species in the macrocycle molecule. Apparently, the presence of the TCNQ molecule favors electric charge transport through SCLC controlled by an exponential trap distribution. Since the contact is ohmic in the vicinity of the electrodes, spatial charges are formed, which oppose current flow through the molecular material films at large enough applied fields, leading to current saturation.

Electrical conductivity was evaluated at 298 K for each device. From the *I–V* data, the electrical conductivity values (σ) for the devices were determined from the following expressions [41]:

$$R = \frac{V}{I} \text{ and } \sigma = \frac{w}{RtL}$$

In these expressions, R is the electrical resistance of the material, t is the thickness of the film, L is the length of the electrodes and w is the distance between the electrodes. The results, which are presented in Table 4, show that the doped semiconductor device has a higher conductivity. Moreover, electrical conductivity values at room temperature for both devices are slightly above the typical range for organic semiconductor materials (10^{-6} to 10^{-1} S·cm^{-1}) [22] and about the middle of such range for inorganic semiconductors (10^{-8} to 10^{3} S·cm^{-1}). This is important because a molecular semiconductor is generally defined in terms of its conductivity at room temperature, which is related to structure, stacking and orbital overlap. Notice as well that the impurities do not seem to affect charge carrier mobility. The value of the band gap, as obtained by the Tauc method and verified by the theoretical calculations, the ease of manufacturing simple thin-film devices of doped molecular semiconductor and the electrical conductivity values at 298 K suggest that the molecular material doped from [Cu(II)TAAB]$^{2+}$ and TCNQ may be useful in organic electronic device production.

5. Conclusions

This work reports the doping of molecular material from the [Cu(II)(TAAB)]$^{2+}$ macrocycle and the TCNQ electronic acceptor. Both IR-spectroscopy results and DFT calculations indicate that the Cu(II) atoms are coordinated to the four nitrogen atoms of the macrocycle along an equatorial orientation, and to one oxygen atom belonging to a water molecule along the axial direction. Water molecules also form hydrogen bonds through their hydrogen atoms: the first one with a terminal nitrogen atom in TCNQ, and the second between one of the terminal hydrogen atoms from the outer phenyl ring of the TAAB and the same terminal nitrogen atom in TCNQ. The films obtained by high-vacuum evaporation show a homogeneous and predominantly amorphous appearance, with the semiconductor molecular material uniformly covering the zone between the source and collector electrodes, and an optical band gap of 2.4 eV (confirmed by DFT calculations). Hydrogen bonds involving the TCNQ molecule have a significant effect on the optical and electrical properties of the system. Changes in the electrical properties are evident when fabricating a bulk heterojunction-type structure, such as *glass/ITO/Cu(II)(TAAB)(H$_2$O)](TCNQ)$_2$/Ag*, which allows us to evaluate its *I–V* behavior both in the dark and in the presence of electromagnetic radiation from bands ranging between IR and UV. The device shows ohmic behavior at low voltages and SCLC at higher voltages; the doped semiconductor material had room-temperature electrical conductivity values similar to those of typical organic semiconductors. These properties suggest that the material could be a suitable candidate for use in complex devices related to the OLED, OFET and OSC families.

Acknowledgments

Maria Elena Sánchez-Vergara gratefully acknowledges the financial support of Universidad Anáhuac México, Campus Norte, under grant INNADBSEVM140129141. The authors wish to thank the technical support of Ing. Guillermo Villagrán, Renata Maya Rangel (Universidad Anáhuac México) and Lemuel Enrique Herrera Covarrubias (Instituto Politécnico Nacional).

References

[1] J. Caro, S. Garelik, A. Figueras, Anisotropic materials prepared by OCVD: organic molecular conductors, Chem. Vap. Depos. 2 (1996) 251–253.
[2] A. Figueras, S. Garelik, J. Caro, J. Cifre, J. Venciana, C. Rovira, E. Ribera, E. Canadell, A. Seffar, Preparation and characterization of conducting thin films of molecular organic conductors (TTF-TCNQ), J. Cryst. Growth 166 (1996) 798–803.
[3] P. Cassoux, D. De Caro, L. Valade, H. Casellas, B. Daffos, M.E. Sánchez Vergara, From molecule-based (super)conductors to thin films, nanowires and nanorings, Mol. Cryst. Liq. Cryst. 380 (2002) 45–52.
[4] T. Mori, Organic conductors with unusual band fillings, Chem. Rev. 104 (2004) 4947–4969.
[5] J. Ferraris, D.O. Cowan, V. Walatka, J.H. Perlstein, Electron transfer in a new highly conducting donor-acceptor complex, J. Am. Chem. Soc. 95 (3) (1973) 948–949.
[6] H. Miyasaka, Control of charge transfer in donor/acceptor metal organic frameworks, Acc. Chem. Res. 46 (2) (2012) 248–257.
[7] A.G. Kolchinski, Anhydrooligomers of o-aminobenzaldehydes - the rich chemistry of the Busch macrocycles, Coord. Chem. Rev. 174 (1998) 207–239.
[8] M.B. Inoue, M. Inoue, Q. Fernando, K.W. Nebesny, Tetracyanoquinodimethane salts of a copper chelate with Tetrabenzo [b,f,j,n][1,5,9,13]tetraazacyclohexadecine: electrical properties and mixed-valence states, J. Phys. Chem. 91 (1987) 527–530.
[9] Z.J. Zhong, N. Matsumoto, H. Ōkawa, S. Kida, Crystal structure and magnetic properties of the heterobinuclear complex $[(CH_3CN)LNi(mnt)]\cdot CH_3CN$ (L = Tetrabenzo [b,f,j,n][1,5,9,13]tetraazacyclohexadecine and mnt = maleonitriledithiolate), J. Chem. Soc. Dalton Trans. (11) (1989) 2095–2097.
[10] V. Katovic, L.T. Taylor, D.H. Busch, Nickel (II) and copper (II) complexes containing new monocyclic and policyclic ligands derived from the cyclotetrameric Schiff base of o aminobenzaldehyde, Inorg. Chem. (3) (1971) 458–462.
[11] S. Kumar, R. Malhotra, K.S. Dhindsa, Nucleophilic addition reactions involving the copper (II) complex of tetrabenzo[b,f,j,n]tetraza-cyclohexadecine(2,3;6,7;10,11;14,15-BZO_4[16]octane-1,5,9,13-N_4), Polyhedron 11 (1992) 1383–1385.
[12] J. Labuda, V. Plaskoñ, V.V. Pavlishchuk, Effect of solvent and strong base on electrochemical and chemical behaviour of copper tetraaza macrocyclic complex, Inorg. Quim. Acta. 146 (1988) 13–18.
[13] A.J. Jircitano, M.C. Colton, K. Bowman, Unique octaiodine configuration in congested macrocyclic ligand complexes, Inorg. Chem. 20 (1981) 890–896.
[14] K.P. Goetz, J. Tsutsumi, S. Pookpanratana, J. Chen, N.S. Corbin, R.K. Behera, V. Coropceanu, C.A. Richter, C.A. Hacker, T. Hasegawa, O.D. Juschescu, Polymorphism in the 1:1 charge-transfer complex DBTTF-TCNQ and its effects on opytical and electronic properties, Adv. Electron. Mater. 2 (2016) 1600203.
[15] D. De Caro, H. Alves, M. Almeida, S. Caillieux, M. Elgaddari, C. Faulmann, I. Malfant, F. Senocq, J. Fraxedas, A. Zwick, L. Valade, Conducting oriented-$[(n\text{-}C_4H_9)_4N]_2[Ni(dcbdt)_2]_5$ and new (BEDT-TTF)$[Ni(dcbdt)_2]$ phases as microcrystalline films, electrodeposited on silicon substrates, J. Mater. Chem. 14 (2004) 2801–2805.
[16] F. Santerre, R. Côté, G. Veilleux, R.G. Saint-Jacques, J.P. Dodelet, Highly photoactive molecular semiconductors: determination of the essential parameters that lead to an improved photoactivity for modified chloroaluminum phthalocyanine thin films, J. Phys. Chem. 100 (1996) 7632–7645.
[17] A.D. Becke, Density functional exchange energy approximation with correct asymptotic behavior, Phys. Rev. A 38 (1988) 3098–3100.
[18] J.P. Perdew, Y. Wang, Accurate and simple analytic representation of the electron-gas correlation energy, Phys. Rev. B 45 (1992) 13244–13249.
[19] M.J. Frisch, G.W. Trucks, H.B. Schlegel, G.E. Scuseria, M.A. Robb, J.R. Cheeseman, G. Scalmani, V. Barone, B. Mennucci, G.A. Petersson, H. Nakatsuji, M. Caricato, X. Li, H.P. Hratchian, A.F. Izmaylov, J. Bloino, G. Zheng, J.L. Sonnenberg, M. Hada, M. Ehara, K. Toyota, R. Fukuda, J. Hasegawa, M. Ishida, T. Nakajima, Y. Honda, O. Kitao, H. Nakai, T. Vreven, J.A. Montgomery Jr., J.E. Peralta, F. Ogliaro, M. Bearpark, J.J. Heyd, E. Brothers, K.N. Kudin, V.N. Staroverov, R. Kobayashi, J. Normand, K. Raghavachari, A. Rendell, J.C. Burant, S.S. Iyengar, J. Tomasi, M. Cossi, N. Rega, J.M. Millam, M. Klene, J.E. Knox, J.B. Cross, V. Bakken, C. Adamo, J. Jaramillo, R. Gomperts, R.E. Stratmann, O. Yazyev, A.J. Austin, R. Cammi, C. Pomelli, J.W. Ochterski, R.L. Martin, K. Morokuma, V.G. Zakrzewski, G.A. Voth, P. Salvador, J.J. Dannenberg, S. Dapprich, A.D. Daniels, Ö. Farkas, J.B. Foresman, J.V. Ortiz, J. Cioslowski, D.J. Fox, Gaussian 09, Revision A.1, Gaussian, Inc., Wallingford CT, 2009.
[20] S. Grimme, J. Antony, S. Ehrlich, H.J. Krieg, A consistent and accurate ab initio parametrization of density functional dispersion correction (DFT-D) for the 94 elements H-Pu, Chem. Phys. 132 (2010), 54104.
[21] V.P. Bansal, P.P. Thankachan, R. Prasad, Catalytic and electrocatalytic wet oxidation of phenol using two new nickel(II) tetraazamacrocycle complexes under heterogeneous conditions, J. Mol. Catal. A Chem. 316 (2010) 131–138.
[22] M.E. Sánchez-Vergara, J. Gómez-Lara, R.A. Toscano, S. Hernández-Ortega, Diaqua tetrabenzo (b,f,j,n) {1,5,9,13} tetraazacyclohexadecine copper (II) and nickel (II) bisanthraflavates; crystal and molecular structure, J. Chem. Crystallogr. 28 (11) (1998) 825–830.
[23] C. Adamo, F. Lelj, A density functional study of bonding of water to copper and nickel atoms, J. Mol. Struct. THEOCHEM 389 (1997) 83–89.
[24] M. Bendikov, F. Wudl, Tetrathiafulvalenes, oligoacenenes, and their buckminsterfullerene derivatives: the brick and mortar of organic electronics, Chem. Rev. 104 (2004) 4891–4945.
[25] R.F.W. Bader, Atoms in Molecules: A Quantum Theory, Oxford University Press, Oxford, 1990.
[26] S.J. Grabowski, What is the covalency of hydrogen bonding? Chem. Rev. 111 (4) (2011) 2597–2625.
[27] J.C. García-Ramos, R. Galindo-Murillo, A. Tovar-Tovar, A.L. Alonso-Saenz, V. Gómez-Vidales, M. Flores-Álamo, L. Ortiz-Frade, F. Cortes-Guzmán, R. Moreno-Esparza, A. Campero, L. Ruiz-Azuara, The π-back-bonding modulation and its impact in the electronic properties of Cu(II) antineoplastic compounds: experimental and theoretical study, Chem. Eur. J. 20 (2014) 13730–13741.
[28] D. Kilvenson, R. Neiman, ESR studies on the bonding in cooper complexes, J. Chem. Phys. 35 (1961) 149–155.
[29] J. Peisach, W.E. Blumberg, Structural implications derived from the analysis of electron paramagnetic resonance spectra of natural and artificial copper proteins, Arch. Biochem. Biophys. 165 (1974) 691–708.
[30] E. Bill, J. Müller, T. Weyhermuller, K. Wieghardt, Intramolecular spin interactions in bis(phenoxyl)metal complexes of zinc(II) and copper(II), Inorg. Chem. 38 (1999) 5795–5802.
[31] M.A. Ali, A.H. Mirza, R.J. Fereday, R.J. Butcher, J.M. Fuller, S.C. Drew, L.R. Gahan, G.R. Hanson, B. Moubaraki, K.S. Murray, Synthetic, EPR spectroscopic, magnetic and X-ray crystallographic structural studies on copper(II) complexes of the tridentate N_2S donor ligand formed from 6 methyl 2 formylpyridine and S methyldithiocarbazate (Hmpsme), Inorg. Chim. Acta 358 (2005) 3937–3948.
[32] M.E. Sánchez-Vergara, E.A. Leyva-Esqueda, C. Álvarez, M. López Reyes, Alan Miralrio, Roberto Salcedo, Influence of TCNQ acceptor on optical and electrical properties of tetrasubstituted allenes films fabricated by vacuum thermal evaporation, J. Mater. Sci. Mater. Electron. 27 (2016) 9900–9910.
[33] A. Rodriguez, M.E. Sánchez-Vergara, V. García-Montalvo, A. Ortiz-Rebollo, J.R. Alvarez-Bada, C. Alvarez-Toledano, Electrical and optical properties of copper and nickel molecular materials with tetrabenzo [b,f,j,n] [1,5,9,13] tetraazacyclohexadecine thin films grown by the vacuum thermal evaporation technique, Spectrochim. Acta A 75 (2010) 479–485.
[34] G. García-Moreno, Organic Semiconductors Pi-conjugated Based in Thiophene. Theoretical Study(Doctoral Dissertation) University of Jaen, Faculty of Experimental Sciences, Department of Physical Chemistry and Analytical, Jaen, Spain, May 31st, 2012 (ISBN: 978-84-8439-683-3).
[35] S. Schindler, D.J. Szalda, Syntheses, structures and properties of copper and nickel complexes of the macrocyclic ligand 5,6,11,12,17,18,23,24 octahydro tetrabenzo[b,f,j,n][1,5,9,13] tetraazacyclohexadecine (H_8TAAB), Inorg. Chim. Acta 228 (1995) 93–101.
[36] N. Laidani, R. Bartali, G. Gottardi, M. Anderle, P. Cheyssac, Optical absorption parameters of amorphous carbon films from Forouhi-Bloomer and Tauc-Lorentz models: a comparative study, J. Phys. Condens. Matter 20 (2008), 015216.
[37] E. Tapavicza, F. Furche, D. Sundholm, Importance of vibronic effects in the UV–vis spectrum of the 7,7,8,8 tetracyanoquinodimethane anion, J. Chem. Theory Comput. 12 (10) (2016) 5058–5066.
[38] T.M. Mok, S.K. O'Leary, The dependence of the Tauc and Cody optical gaps associated with hydrogenated amorphous silicon on the film thickness: αl experimental limitations and the impact of curvature in the Tauc and Cody plots, J. Appl. Phys. 102 (2007), 113525.
[39] F. Urbach, The long-wavelength edge of photographic sensitivity and of the electronic absorption of solids, Phys. Rev. 92 (1953) 1324.
[40] A.J. Heeger, 25th anniversary article: bulk heterojunction solar cells: understanding the mechanism of operation, Adv. Mater. 26 (2014) 10–28.
[41] F.M. Smits, Measurement of sheet resistivities with the four-point probe, Bell Syst. Tech. J. 37 (3) (1958) 711–718.